

GT2011-46471

ROTOR DYNAMIC PERFORMANCE OF AN OIL-FREE TURBO BLOWER FOCUSING ON LOAD CAPACITY OF GAS FOIL THRUST BEARINGS

Tae Ho Kim
Senior Research Scientist
Energy Mechanics Center, Korea Institute of Science and Technology
39-1 Hawolgok-dong, Songbuk-gu, Seoul, Korea, 136-791

Yong-Bok Lee
Principal Research Scientist

Tae Young Kim
Research Engineer
Maritime Research Institute, Hyundai Heavy Industries. Co. LTD
1 Jeonha-dong, Dong-gu, Ulsan, Korea, 687-792

Kyong Ho Jeong
Principal Researcher
Rotating machinery group, Hwang Hae Electric
679-1, Gojan-Dong, Namdong-Gu, Incheon Metropolitan city, Korea, 405-819

ABSTRACT

Engineered design of modern efficient turbomachinery based on accurate model predictions is of importance as operating speed and rate power increase. Industrial applications use hydrodynamic fluid film bearings as rotor support elements due to their advantages over rolling element bearings in operating speed, system stability (rotordynamic and thermal), and maintenance life. Recently, microturbomachinery (<250 kW) implement gas foil bearings (GFBs) as its rotor supports due to its compact design without lubricant supply systems and enhanced stability characteristics. To meet the needs from manufacturers, the turbomachinery development procedure includes a rotordynamic design and a gas foil journal bearing (GFJB) analysis in general. The present research focuses on the role of gas foil thrust bearings (GFJBs) supporting axial load (static and dynamic) in an oil-free turbo blower with a 75kW (100 HP) rate power at 30,000 rpm. The turbo blower provides a compressed air with a pressure ratio of 1.6 at a mass flow rate of 0.92 kg/s, using a centrifugal impeller installed at the rotor end. Two GFJBs with a diameter of 66mm and a length of 50mm and one pair of GFTB with an outer diameter of 144 mm and an inner diameter of 74 mm support the rotor with an axial length of 493 mm and a weight of 12.7 kg. A finite element rotordynamic model prediction using predicted linearized GFJB force coefficients designs the rotor-GFB system with stability at the rotor speed of 30,000 rpm. Model predictions of the

GFTB show axial load carrying performance. Experimental tests on the designed turbo blower, however, demonstrate unexpected large amplitudes of subsynchronous rotor lateral motions. Post-inspection reveals minor rubbing signs on the GFJB top foils and significant wear on the GFTB top foil. Therefore, GFTB is redesigned to have the larger outer diameter of 166 mm for the enhanced load capacity, i.e., 145%, increase in its loading area. The modification improves the rotor-GFB system performance with dominant synchronous motions up to the rate speed of 30,000 rpm. In addition, the paper studies the effect of GFTB tilting angles on the system performance. Insertion of shims between the GFTB brackets changes the bearing tilting angles. Model predictions show the decrease in the thrust load capacity by as large as 86 % by increase in the tilting angle to 0.0006 radian (0.03438 deg). Experimental test data verify the computational model predictions.

INTRODUCTION

The implementation of gas foil bearings (GFBs) into high speed turbomachinery has advantages over traditional bearings including higher rotating speed, better reliability, and low maintenance cost without lubrication systems [1]. GFBs operate under self-acting hydrodynamic principles in the same manner as conventional sleeve type rigid hydrodynamic bearings. However, compliant surfaces generated by bump/leaf

foil layers increase the load capacity relative to rigid bearings and permit operations at both extremely high and low temperatures [2].

Due to the increasing needs of high speed and high power turbomachinery, gas foil thrust bearings (GFTBs) become critical mechanical components which are expected to support large axial forces. Heshmat et al. [3] first develop a numerical prediction model of GFTBs using the finite difference method and reveal that the inclined plane of the top foil plays an important role in generating the pressure gradient. Later, Ref [4] introduces the advanced model of GFTBs using the finite difference method for the gas film flow analysis and the finite element method for the bump structural stiffness analysis. Jordanoff [5] proposes an optimal air film profile for the maximum load capacity of gas thrust bearings. The study assumes the high compressibility number up to 1000. Later, the same author [6] develops simple analytical equations producing the local bump compliances both at the fixed-bump and free conditions. Using the simple equations, the static performances of GFTBs are easily predicted. Reference [7] predicts the effects of tilting angles on static performance of GFTBs. Note that bearing misalignment or manufacturing inaccuracy may cause tilting angles of GFTBs when implemented into actual turbomachinery. The predictions reveal that little changes in the tilting angle can reduce the GFTB load capacity significantly.

Recently, DellaCorte and Bruckner [8] introduce the design, fabrication, and performance test process of simple GFTBs. Using the advanced tooling process, the multistage bump foil layer can have varying stiffness coefficients in the radial direction. Experimental test data of bearing torque versus static load demonstrate the reliable operation of the manufactured GFTBs.

References [9-11] implement GFJBs as well as GFTBs into industrial applications, i.e., turbo compressors [9,10] and turbo blower [11]. Rotordynamic performance of test bearings are measured in aerodynamic surge conditions which verify the reliable operations of the 75 kW (100 Hp) oil-free systems in Refs. [9,11]. Recently, Ref. [10] presents the rotordynamic performance measurements of a 225 kW (300 Hp) oil-free turbo compressor operating at 60 krpm. The paper also provides model predictions in good agreement with the experimental measurements.

The present paper shows an advancement in the rotor-GFB system performance of a 75 kW oil-free turbo blower. A linear rotordynamic model designs the oil-free system for increasing rotor speed, and experimental rotor speed-up tests verify the model predictions with a focus on the load carrying capacity of GFTBs with tilting angles.

DESCRIPTION OF 75 KW TURBO BLOWER

Figure 1 shows a schematic view of the 75 kW (100HP) oil-free turbo blower with a rotor supported on gas foil bearings (GFBs). The turbo blower rated speed is 30 krpm (500 Hz). Two GFJBs and one pair of GFTBs support radial and axial loads, respectively. The rotating part of the turbo blower consists of a single centrifugal impeller, a main shaft with a permanent magnet, a thrust runner, and a cooling fan. The total length of the rotating part and the diameter of the main shaft are 493 mm and 66 mm, respectively. The cooling fan and thrust runner are located at the opposite end of the centrifugal

impeller for a mass balance of the rotating part. The cooling fan makes a cooling flow passing the motor core and outer surfaces of the GFJBs and GFTBs housing, thus removing heat generated in the driving motor (rotor and stator) and the support bearings.

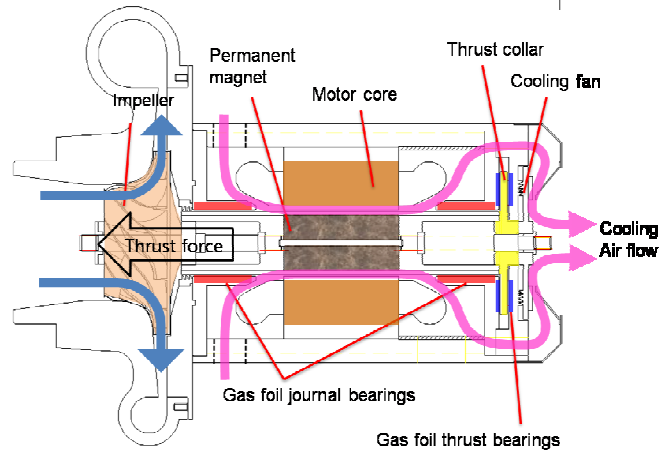


Fig.1 Oil-free 75 kW (100 HP) turbo blower. Rated speed of 30 krpm (500 Hz).

The aerodynamic design of the centrifugal impeller with splitter blades, diffuser, and volute has been conducted. Figure 2 displays a three dimensional (3-D) model of the centrifugal impeller designed using CFD analysis. The figure shows one eighth (1/8) sectional area of the whole analysis domain. Table 1 lists the design parameters of the oil-free turbo blower. The blower has the pressure ratio of 1.6 and mass flow rate of 0.92 kg/sec at the rated speed of 30 krpm. Due to the single impeller configuration, the calculated net force along the axial direction is quite large, i.e., 503.8 N. The direction of the axial (thrust) force is denoted in Fig. 1. Note that for aerodynamically symmetric configuration the manufacturer designs oil-free turbo blowers with two identical impellers at both rotor ends. In the case, the axial forces are well balanced, i.e., nearly null net force along the axial direction, although the manufacturing cost increases.

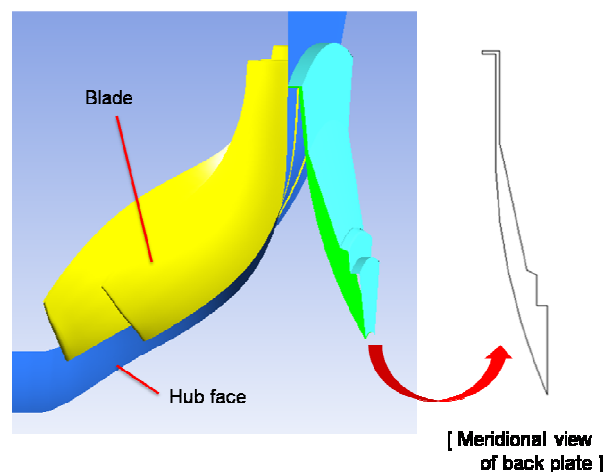


Fig. 2 Three dimensional (3-D) view of centrifugal impeller design developed using CFB analysis. one eighth (1/8) sectional area of whole analysis domain. Provided by manufacturer.

Table 1. Design parameters of the oil-free turbo blower.

Parameters	Value	Unit
Gas	Air	-
Pressure ratio (total to total)	1.6	-
Mass flow rate	0.92	kg/sec
Inlet flow conditions	Standard atmosphere	-
Rate rotational speed	30,000	rpm
No. of blade (main + split)	8 + 8	ea
Net thrust force	503.8	N

Figure 3 shows GFJB and GFTB used in the oil-free turbo blower. The GFJB with a diameter of 66 mm has a single top foil and a single bump layer. The GFTB with inner and outer diameters of 74 mm and 144 mm, respectively, has eight top foils and eight bump layers. The top foils have MoS₂ solid lubricants coated with a thickness of 0.020 mm on the upper surface. Table 2 provides detailed design parameters of the GFJB and GFTB.

ROTOR DYNAMIC ANALYSIS OF TURBO BLOWER SHAFT SUPPORTED ON GAS FOIL BEARINGS

Figure 4 presents the finite element (FE) rotordynamic model of the oil-free turbo blower shaft. The total number of the FEs is 73 and the aspect ratios (length over diameter) of all FEs are smaller than 0.2. The model includes two GFJBs with linearized dynamic coefficients (stiffness and damping). The total shaft mass of 12.7 kg imposes static loads of 54.2 N and 52.2 N on the impeller end GFJB and the thrust runner end GFJB, respectively. Appendix A provides the synchronous stiffness and damping coefficients versus speed for the GFJBs, which were predicted using the computational model in Ref. [12]. A transfer matrix method (TMM) based rotordynamics tool predicts the damped eigenvalues and logarithmic decrement of the rotordynamic model for increasing rotor speed.

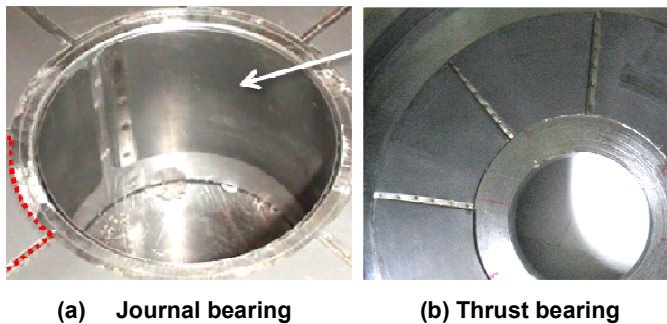
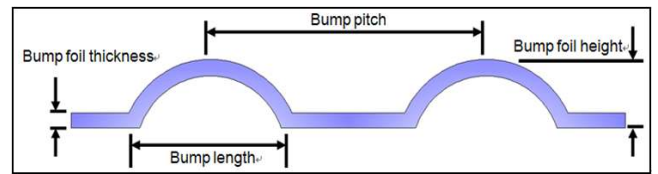


Fig. 3 Gas foil bearings. (a) Journal bearing (GFJB) with a single top foil and a single bump layer. (b) Thrust bearing (GFTB) with eight top foils and eight bump layers.

Table 2. Design parameters of GFJB and GFTB

Gas foil journal bearing (GFJB)	
Bearing radius	33.00 mm
Bearing length	50.00 mm
Bearing radial clearance	0.15 mm
Top foil thickness (including MoS ₂ Coating, 0.02 mm)	0.22 mm
Bump foil thickness	0.20 mm
Bump height	0.52 mm
Bump pitch	5.00 mm
Bump length	2.66 mm
Foil material	Stainless steel
Gas foil thrust bearing (GFTB)	
Outer radius	72.00 mm
Inner radius	37.00 mm
Bearing axial clearance	0.15 mm
Top foil thickness (including MoS ₂ Coating, 0.02 mm)	0.22 mm
Bump foil thickness	0.20 mm
Bump height	0.50 mm
Bump pitch	5.00 mm
Angle of inclined part*	17.5 °
Number of top foils	8
Foil material	Stainless steel



*Denoted in Fig 14. See also Ref. [3,7] for the definition of the angle of included part

Axial length of model : 493 mm
 Total mass of rotor : 12.7 Kg
 Interconnection element : two gas foil journal bearings
 Number of total stations : 73

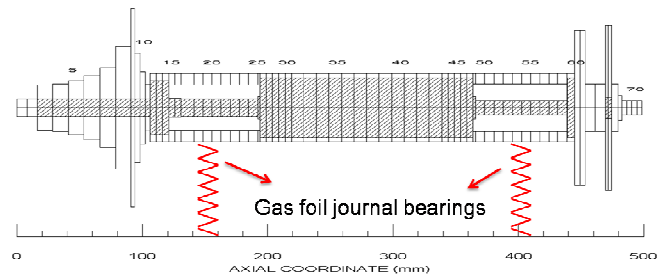


Fig.4 Finite element (FE) model of oil-free turbo blower rotor-GFBs system.

Figure 5 shows predicted natural frequency versus rotor speed, and Fig. 6 presents predicted logarithmic decrement versus rotor speed. The first two natural frequencies for the cylindrical and conical rigid body modes are denoted. In general, the predicted cylindrical mode natural frequency changes little against rotor speed, but the predicted conical mode natural frequency decreases rapidly as the rotor speed increases. Figure 6 illustrates the mode shapes at 30 krpm. The predicted cylindrical and conical mode natural frequencies due to the synchronous rotor motion (1X rotor speed) are located below 5 krpm (83 Hz) and at ~ 11 krpm (183 Hz), respectively. The figure also shows the predicted natural frequencies due to the half synchronous speed (1/2X rotor speed) at ~ 5 krpm (83 Hz) and ~18 krpm (300 Hz) for the cylindrical and conical modes, respectively. Note that the third natural frequency for the rotor bending mode higher than 65 krpm (1,083 Hz) is omitted for brevity. The predicted logarithmic decrements for both the cylindrical and conical mode natural frequencies higher than zero until 40 krpm imply stable operation of the rotor – GFB system up to the rated speed of 30 krpm with a speed margin of 33%.

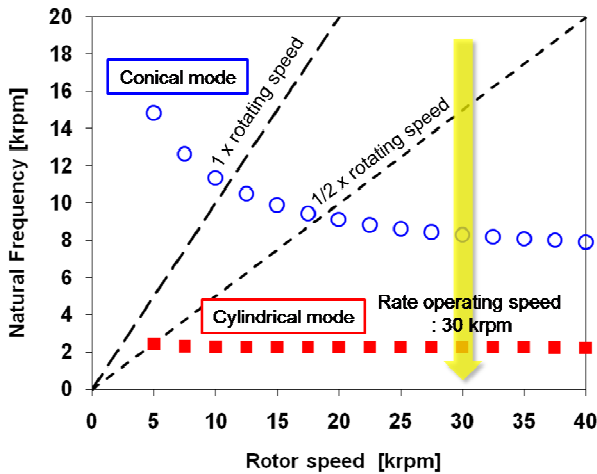


Fig. 5 Predicted natural frequency versus rotor speed. Cylindrical and conical mode natural frequencies denoted.

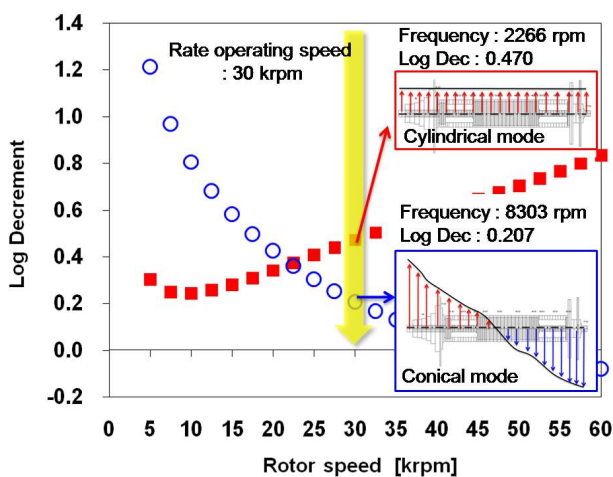


Fig. 6 Predicted logarithmic decrement versus rotor speed. Cylindrical and conical mode natural frequencies denoted. Mode shapes illustrated at 30 krpm.

EXPEREMENTAL TESTS

Figure 7 shows a schematic view of the developed 75 kW oil-free turbo blower with four eddy current sensors installed. Two pairs of orthogonally positioned eddy current sensors with a sensitivity of $70 \mu\text{m/V}$ measure shaft motions in the vertical and horizontal directions at both the shaft ends. Note that the shaft has small sensor target caps with a diameter of 18 mm installed at both the shaft ends. As the rotor speed increases to 18 krpm (300 Hz) and coasts down to rest, Fig. 8 show waterfall plot of the rotor response amplitude at the rotor thrust runner end in the vertical direction. From 12 krpm (200 Hz) to 15 krpm (250 Hz), subsynchronous rotor motions at half rotor speed frequency (1/2X) arise from 90 Hz to 120 Hz. Above the rotor speed, the figure shows unexpected widespread excitation frequencies with small amplitudes, thus implying rotor rubbing. Note also large amplitudes of subsynchronous motions at the fixed frequency of ~ 100 Hz above 15 krpm.

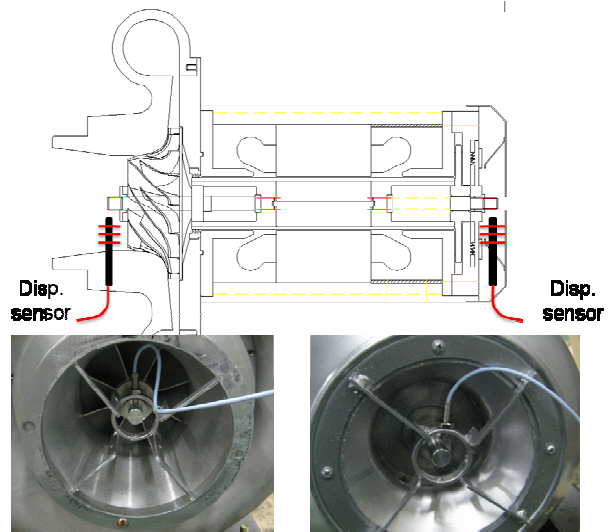


Fig. 7 Schematic view of developed 75 kW oil-free turbo blower (upper) with four eddy current sensors installed (lower in photos).

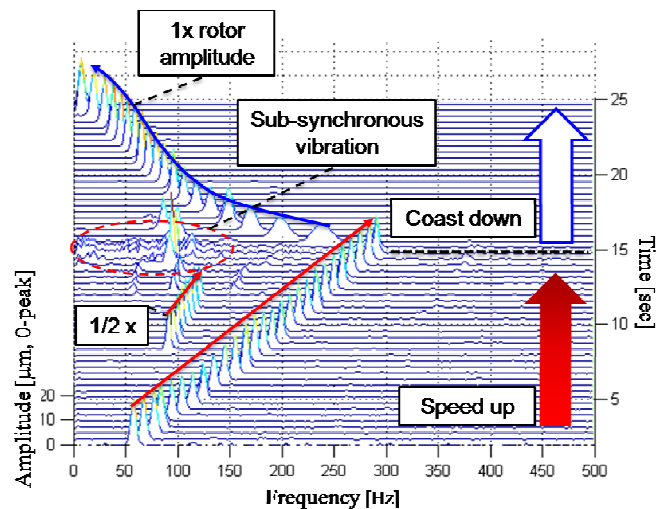


Fig. 8 Waterfall plot of rotor response amplitude measured at rotor thrust runner end in vertical direction. Speed up from 3 krpm to 18 krpm and coastdown to 0 rpm.

A post inspection of the GFJBs reveals minor wear on the top foil surface. The motor side GFTB has significant wear marks on the top foil surface, while the cooling fan side GFTB in the opposite face shows little wear marks as shown in Fig. 9. Note the relative positions of the pair of the GFTBs with respect to the impeller (thrust force) direction denoted in Fig. 9. From the significant wear marks on all eight top foil surfaces of the motor side GFTB, it is thought that the GFTB has lower load capacity than expected, thus failing to support the unbalanced axial force of 503.8 N shown in Table 1.

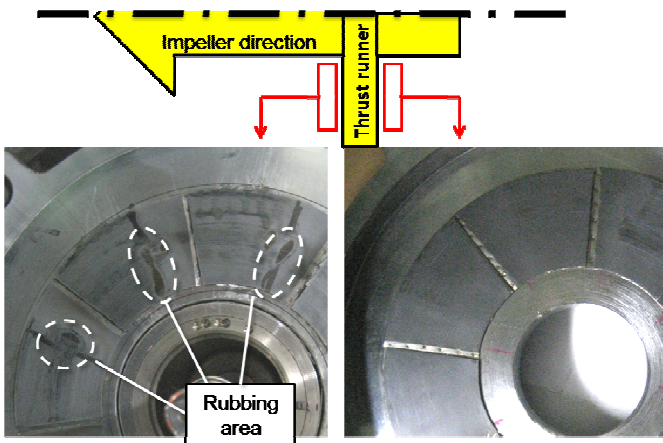


Fig. 9 Photos of GFTB top foil surfaces after test to 18 krpm. Motor side GFTB (left) and cooling fan side GFTB (right).

Figure 10 presents the predicted load capacity versus rotor speed for the test GFTB with the outer radius of 72 mm, as listed in Table 2. The predicted thrust load capacity of the GFTB at 30 krpm is 549 N which is higher than the turbo blower axial unbalance force of 503.8 N by ~ 10 %. The predicted thrust load capacity reduces to 300 N at the rotor speed of 17.5 krpm. Note that presently the maximum load capacity of test GFTB is predicted at the minimum film thickness of 5 μm . The (original) test GFTB is modified to have an increased outer radius of 83 mm for an increase in the thrust load capacity. Note that the corresponding increase in the thrust loading area is ~ 145%. The predicted load capacity of the modified GFTB with the radius of 83 mm versus rotor speed is also displayed in Fig. 10. Note that the maximum load capacity at the top speed of 30 krpm increases from 549 N to 1,028 N, i.e., ~ 90 % increment. Figure 11 shows the modified GFTB with the increased outer radius. Note that the radius of the original thrust runner with an outer radius of 75 mm is also modified to 85 mm although the photo of the thrust runner is omitted for brevity.

A speed-up and coastdown test is conducted for the modified GFTB configuration. Figure 12 shows waterfall plot of the rotor response amplitude for the modified GFTB with the outer radius of 83 mm. The measurements are taken at the rotor thrust runner end in the vertical direction during rotor speed-up test from 0 krpm to 30 krpm. The test results show dominant synchronous (1X) rotor response amplitudes with relatively smaller amplitudes of subsynchronous motions at the fixed frequency of 140 Hz, thus implying an improvement in the rotor-GFB system performance.

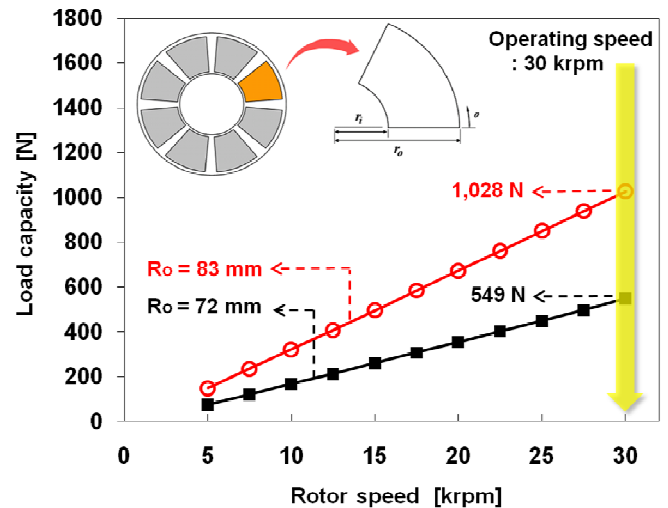


Fig. 10 Predicted GFTB load capacity versus rotor speed for two GFTB outer radii of 72 mm (original) and 83 mm (modified). Load capacities predicted at minimum film thickness of 5 μm .

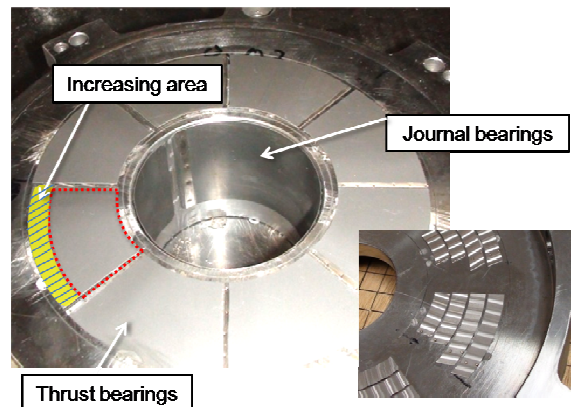


Fig. 11 Modified GFTB with increasing outer radius of 83 mm.

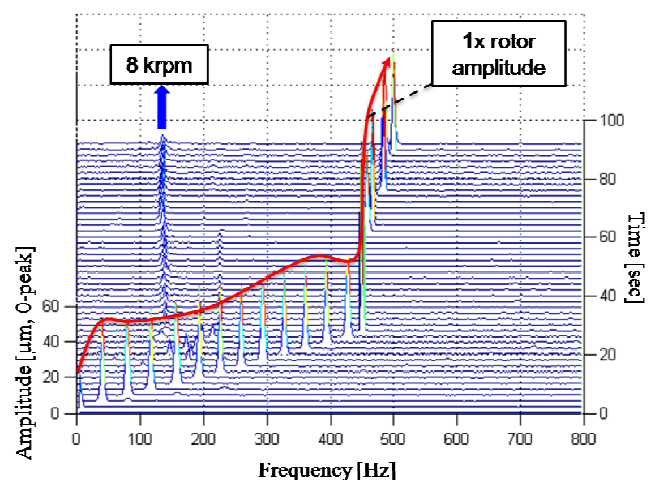


Fig. 12 Waterfall plot of rotor response amplitude measured at rotor thrust runner end in vertical direction for modified GFTB configuration with outer radius of 83 mm. Speed up from 0 krpm to 30 krpm.

EFFECT OF GFTB TILTING ANGLES

In addition, the present paper studies the effect of GFTB tilting angles on the thrust load capacity. Note that Ref. [7] points out a reduction in the predicted load capacity of a GFTB with tilting angles. Figure 13 illustrates the GFTB with null tilting angle (upper) and with tilting angle of θ° (lower). In the present turbo blower system, the tilting angles are applied by insertion of shims between the GFTB back plates (motor side and cooling fan side) facing each others.

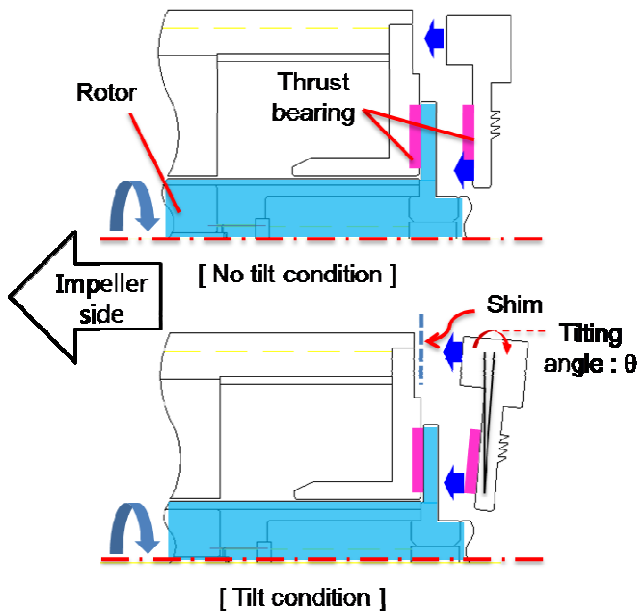


Fig. 13 GFTB tilting conditions. Null tilting angle (upper) and tilting angle of θ° (lower). Tilting angles applied by installation of shims between GFTB back plates.

For the modified GFTB with the outer radius of 83 mm, Fig. 14 shows the predicted load capacity versus GFTB top foil number for increasing GFTB back plate tilting angles (θ) of 0.0 radian (0.0 deg), 0.0002 radian (0.01146 deg), and 0.0006 radian (0.03438 deg) at the rotor speed of 30 krpm. The computational model is detailed in Ref. [7]. Note that test GFTB has tilting angles (θ) of 0.0002 radian (0.01146 deg) and 0.0006 radian (0.03438 deg) by inserting shims with thicknesses of 30 μm and 90 μm , respectively, at the angular location of the top foil number 1 as shown in Fig. 14. Without tilting angle the GFTB has the maximum load capacity of 1,023 N with 128 N for each top foil. With the tilting angle of 0.0002 radian (0.01146 deg), the load capacities for the top foils reduce significantly, particular for the top foils near the top foil number 5. The resultant overall load capacity, i.e., total sum of the load capacities for each top foil is 373 N. The further increase in the tilting angle to 0.0006 radian (0.03438 deg) decreases the GFTB load capacity to 144 N, i.e., 86 % decrement when compared to the maximum load capacity of 1,023 N with null tilting angle. Note asymmetric thrust load distributions along the axis passing the top foil numbers 1 and 5 due to the geometrically asymmetric positioning of the inclined and flat planes of the top foils along the same axis.

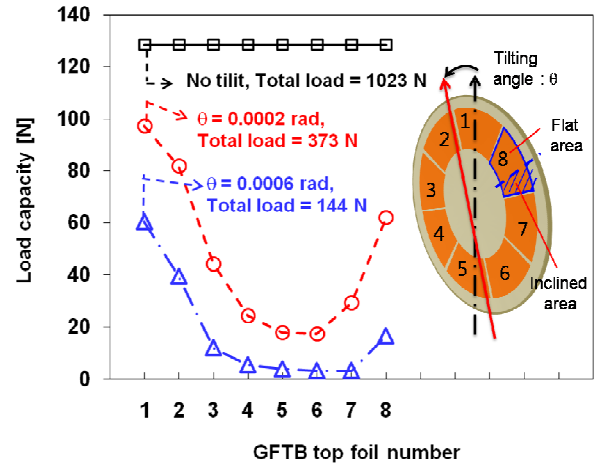


Fig. 14 Load capacity versus GFTB top foil number for increasing GFTB back plate tilting angles (θ) of 0.0 radian (0.0 deg), 0.0002 radian (0.01146 deg), and 0.0006 radian (0.03438 deg). Rotor speed of 30 krpm.

For the modified GFTB configuration with the outer radius of 83 mm, Figs. 15 and 16 show waterfall plots of rotor response amplitudes measured at the rotor thrust runner end in the vertical direction for the GFTB back plate tilting angles (θ) of 0.0002 radian (0.01146 deg) and 0.0006 radian (0.03438 deg), respectively. During the speed-up test to 16 krpm (267 Hz) in Fig. 15, the rotor has significant subsynchronous motions at the widespread excitation frequencies with peak amplitudes near 100 μm arising from the rotor speed of 13 krpm (217 Hz) for the tilting angle (θ) of 0.0002 radian (0.01146 deg). With the further increase in the tilting angle to 0.0006 radian (0.03438 deg), the onset speed of subsynchronous motions decreases to 9 krpm (150 Hz). It is thought that the decrease in the GFTB load capacity by changing the tiling angle causes the rotor rubbing on the GFTB and excites the broad range of frequencies, thus inducing large amplitudes of the subsynchronous motions, in particular near the rotor-GFTB system natural frequency ~ 100 Hz.

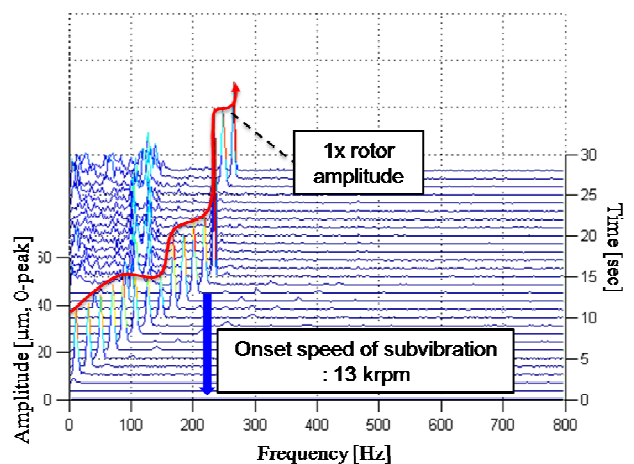


Fig.15 Waterfall plot of rotor response amplitude measured at rotor thrust runner end in vertical direction for modified GFTB configuration with outer radius of 83 mm. GFTB back plate tilting angles (θ) of 0.0002 radian (0.01146 deg). Speed up from 0 krpm to 16 krpm.

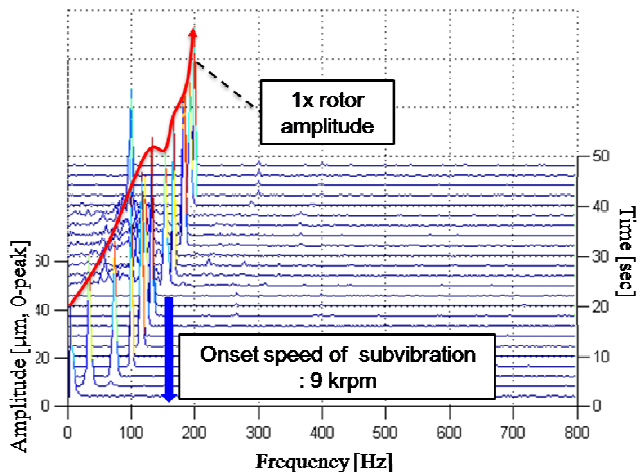


Fig. 16 Waterfall plot of rotor response amplitude measured at rotor thrust runner end in vertical direction for modified GFTB configuration with outer radius of 83 mm. GFTB back plate tilting angles (θ) of 0.0006 radian (0.03438 deg). Speed up from 0 krpm to 12 krpm.

CONCLUSIONS

The paper presents the advancement in the rotor-GFB system performance of the 75 kW oil-free turbo blower. A linear rotordynamic model of the shaft-GFBs system predicts the damped eigenvalues and logarithmic decrement for increasing rotor speeds. The analysis shows stable rotor operations up to the top speed of 30 krpm. However, the experimental test demonstrates subsynchronous rotor motions at widespread frequencies from the rotor speed of 12 krpm (200 Hz). The post inspection reveals significant wear on the top foil surface of the motor side GFTB with minor wear on the top foil surface of the GFJBs, thus implying the lack of the thrust load capacity in the axial direction. Although the original GFTB with outer diameter of 74 mm is predicted to have enough thrust load capacity of 549 N which is larger than the axially acting impeller force of 503.8 N by $\sim 10\%$, it is modified to have a larger radius of 83 mm. The increase in the GFTB outer radius to 83 mm predicts the thrust load capacity of 1,028 N, i.e., $\sim 90\%$ increment. The repeated speed-up tests show dominant synchronous (1X) rotor response amplitudes with negligible subsynchronous motions, thus implying the improvement in the rotor-GFB system performance. In addition, the paper studies the effect of the GFTB tilting angles. The predicted thrust load capacity of test GFTB decreases significantly with increasing GFTB tilting angles. With the tilting angle of 0.0006 radian (0.03438 deg), the load capacity of the GFTB decreases to 144 N, i.e., 86% decrement when compared to the load capacity of 1,023 N with null tilting angle, for example. Experimental tests demonstrate that the onset speed of subsynchronous motions due to the rotor rubbing decreases with the increasing GFTB tilting angles, thus verifying the model predictions.

One of the future researches may include a rotordynamic model development to predict the effect of GFTB statics and dynamics on the radial motion of a rotor supported on GFJBs. Force and moment balance equations including axial and radial reaction forces from GFTBs and GFJBs, respectively, will determine the dynamics of rotor motions, for example.

ACKNOWLEDGMENTS

This material is based upon the works supported by Hwang Hae Electric Company, research project on oil-free turbo blowers, and Korea Institute of Science and Technology (KIST), Research Project: R&D on Power Generation and Energy Storage Technology for Tri-Gen System. The authors thank to researchers at Hwang He Electric Company for their help in preparing the turbo blower test setup.

REFERENCES

- [1] Agrawal, G. L., 1997, "Foil Air/Gas Bearing Technology—An Overview," ASME Paper No. 97-GT-347.
- [2] DellaCorte, C., and Valco, M., J., 2000, "Load Capacity Estimation of Foil Air Journal Bearings for Oil-Free Turbomachinery Applications," STLE Tribol. Trans., **434**, pp. 795–801.
- [3] Heshmat, H., Walowit, J. A., and Pinkus, O., 1983, "Analysis of Gas Lubricated Compliant Thrust Bearings," Journal of Lubrication Technology, **105**, pp 638–646.
- [4] Heshmat, C. A., Xu, D., and Heshmat, H., 2000, "Analysis of Gas Lubricated Foil Thrust Bearings Using Coupled Finite Element and Finite Difference Methods," ASME J. Tribol., **122**, pp. 199–204.
- [5] Iordanoff, I., 1998, "Maximum Load Capacity Profiles for Gas Thrust Bearings Working Under High Compressibility Number Conditions," ASME J. Tribol., **120**, pp. 571–576.
- [6] Iordanoff, I., 1999, "Analysis of an Aerodynamic Compliant Foil Thrust Bearing: Method for a Rapid Design," ASME J. Tribol., **121**, pp. 816–822.
- [7] Park, D. J., Kim, C. H., Jang, G. H., and Lee, Y. B., 2008, "Theoretical Considerations of Static and Dynamic Characteristics of Air Foil Thrust Bearing With Tilt and Slip Flow," Tribol. Intl., **41**, pp. 282–295.
- [8] DellaCorte, C., and Bruckner, R., 2008, "Design, Fabrication, and Performance of Foil Gas Thrust Bearings for Microturbomachinery Applications," NASA TM-215062.
- [9] Lee, Y. B., Kim, T. H., Kim, C. H., and Lee, N. S., 2003, "Suppression of Subsynchronous Vibrations Due to Aerodynamic Response to Surge in a Two-stage Centrifugal Compressor with Air Foil Bearings," STLE Tribol. Trans., **46**, pp. 428–434.
- [10] Lee, Y. B., Jo, S. B., Kim, T. Y., Kim, C. H., and Kim, T. H., 2010, "Rotordynamic Performance Measurement of an Oil-Free Turbocompressor supported on Gas Foil Bearings," IFToMM 8th International Conf. on Rotor Dynamics, Seoul, Korea.
- [11] Kim, K. S., and Lee, I., 2007, "Vibration Characteristics of a 75 kW Turbo Machine With Air Foil Bearings," ASME J. Eng. Gas Turbines Power, **129**, pp. 843–849.
- [12] Lee, Y. B., Park, D. J., Kim, C. H., Kim, S. J., 2008, "Operating Characteristics of the Bump Foil Journal Bearings with Top Foil Bending Phenomenon and Correlation among Bump Foils," Tribol. Intl., **41**, pp. 221–233.

APPENDIX A. SYNCHRONOUS STIFFNESS AND DAMPING COEFFICIENTS VERSUS ROTOR SPEED FOR GFJBs AT IMPELLER AND THRUST RUNNER ENDS.

Figure A1 and Fig. A2 present GFJB synchronous stiffness coefficient versus speed and GFJB synchronous damping coefficient versus speed, respectively. As the rotor speed increases, the amplitudes of the predicted direct stiffness and damping coefficients in the vertical direction (K_{xx} , C_{xx}) decrease. The amplitudes of the direct stiffness and damping coefficients in the horizontal direction (K_{yy} , C_{yy}) are smaller than those in the vertical direction (K_{xx} , C_{xx}) with insignificant changes for increasing speeds.

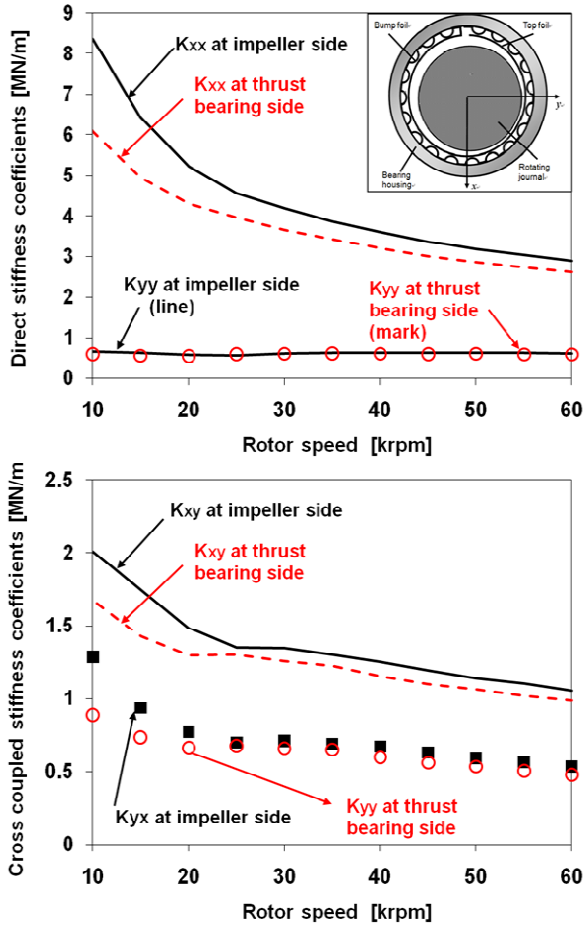


Fig. A1 GFJB synchronous stiffness coefficient versus speed

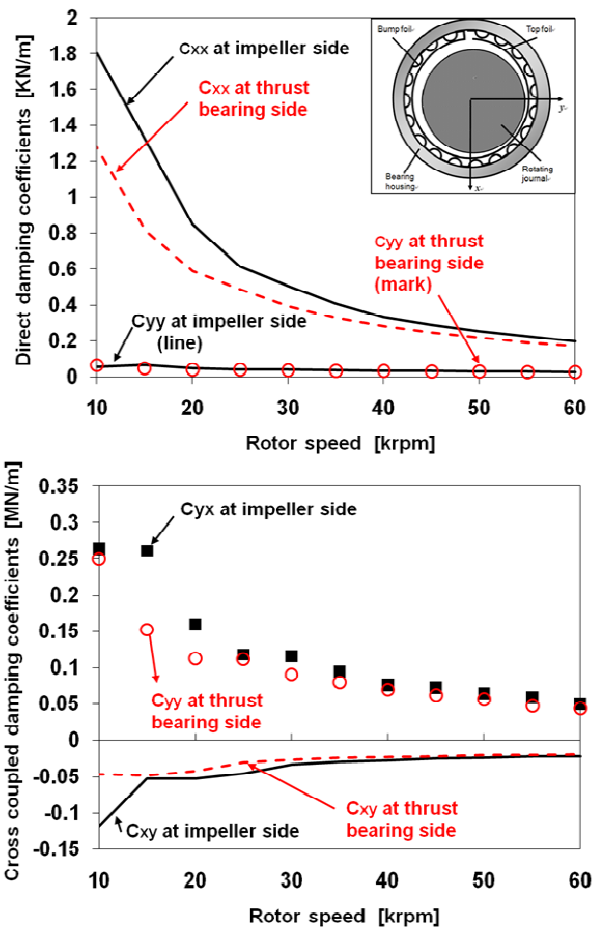


Fig. A2 GFJB synchronous damping coefficient versus speed